Journal of Applied Electrochemistry (2005) 35:499–506
DOI 10.1007/s10800-005-0291-1

3-Hydroxybenzoic acid as AISI 316L stainless steel corrosion inhibitor in a H_2SO_4–HF–H_2O_2 pickling solution

L. NARVÁEZ[1], E. CANO[2,*] and D. M. BASTIDAS[3]
[1]*Metallurgical Institute, UASLP, Avda. Sierra Leona 550, 78210, San Luis Potosí, Mexico*
[2]*CENIM-National Centre for Metallurgical Research, CSIC, Avda. Gregorio del Amo 8, 28040, Madrid, Spain*
[3]*ICMAB-Materials Science Institute of Barcelona, CSIC, Campus Autonoma University of Barcelona, 08193, Bellaterra, Barcelona, Spain*
*(*author for correspondence, e-mail: ecano@cenim.csic.es)*

Received 27 June 2003; accepted in revised form 16 December 2004

Key words: stainless steel, 3-hydroxybenzoic acid, pickling solution, Frumkin adsorption isotherm, projected molecular area

Abstract

3-Hydroxybenzoic acid (3-HBA) was studied for possible use as a AISI 316L stainless steel (SS) corrosion inhibitor in an environmental-friendly aqueous pickling solution of 75 g l^{-1} sulphuric acid (H_2SO_4), 25 g l^{-1} hydrofluoric acid (HF) and 30 g l^{-1} hydrogen peroxide (H_2O_2). 3-HBA was tested in concentrations from 5×10^{-5} to 5×10^{-1} M at 298 and 313 K temperature. Inhibition efficiency increased with the 3-HBA concentration. The inhibitor mechanism is discussed in terms of the properties of the isotherm equations of Frumkin, Hill-de Boer and Kastening–Holleck mainly. The shape, the trend of the slopes along the curve and the existence of inflection points, were analysed as the characteristics that differentiate one adsorption equation from another. The best fit was obtained using the Frumkin isotherm model. The projected molecular area of 3-HBA was calculated as a structural parameter to elucidate its optimal inhibition mechanism.

1. Introduction

Austenitic stainless steels (SS) are widely used in many applications where high corrosion resistance is required, such as in the petrochemical and pharmaceutical industries, industrial power generation and desalination plants. However, certain factors in the handling or manufacturing of these alloys can make them susceptible to localised corrosion and affect their performance. A clean, uniform and corrosion-resistant surface is not only desirable in some services but can also be an absolute necessity. Cleaning and pickling remove foreign materials and promote stability, achieving a uniform surface that is resistant to localised corrosion. SS passivation favours corrosion resistance by forming a protective oxide film [1].

Pickling processes include scale removal, complete dissolution of chromium-depleted alloy (resulting from the migration of chromium from the SS surface into the oxide film), and recovery of the highest surface passivity compatible with the alloy's chemical analysis. The localised corrosion resistance of the final SS product is negatively affected by the presence of a residual chromium-depleted layer.

A nitric (HNO_3)-hydrofluoric (HF) acid mixture is the pickling solution most widely used by SS equipment manufacturers and serves to remove both metallic contamination and welding and heat-treatment scales. HNO_3-HF mixtures, typically 10–15% nitric acid and 2–4% hydrofluoric acid, often also include sulphuric (H_2SO_4) or hydrochloric (HCl) acids and/or pickling accelerating additives such as wetting agents, emulsifiers, surfactants and inhibitors [2].

Pickling is among the most hazardous processes for the environment since it involves the emission of NO_x fumes, characterised by their reddish colour; mainly nitrogen monoxide (NO) and nitrogen dioxide (NO_2). Due to the air pollution that they create, NO_x gases are subject to a maximum permitted emission limit of 160 ppm [3, 4]. Nitric acid, its fumes, and other nitrogen oxides all possess a high level of toxicity [5, 6], making it necessary to use scrubbing towers and subsequently neutralise the strong acids formed. A second problem associated with the use of nitric acid is that of water pollution and the disposal of spent liquors and sludge from the bath.

Mixtures of sulphuric acid and hydrogen peroxide (H_2O_2) are used in SS pickling because they present a

number of advantages, including low waste treatment cost, reduced attack on the metal surface, and the ability to operate in continuous (as well as batch) mode. This new procedure seeks to eliminate the production of NO_x.

The aim of this paper is to study the corrosion inhibition mechanism of 3-hydroxybenzoic acid (3-HBA) for AISI 316L SS in a H_2SO_4–HF–H_2O_2 aqueous solution mixture, based on analysis of the properties of the Langmuir, Frumkin, Hill-de Boer, Parsons, Damaskin–Parsons, Kastening–Holleck, Flory–Huggins, Dhar–Flory–Huggins and Bockris–Swinkels isotherms. The paper is completed by calculating the surface area of 3-HBA based on the projected molecular area.

2. Experimental

Tests were performed using a commercial AISI 316L austenitic SS (UNS SS31603), <0.0039 C wt%, ≤ 0.75 Si, ≤2.20 Mn, 0.040 P, 0.015 S, 17.8 Cr, 12.5 Ni, 2.8 Mo and the balance Fe. Specimens of 50 mm×25 mm were mechanically cut from a 2.0 mm thick sheet, decreased with acetone and dried at room temperature.

Eleven concentrations of 3-HBA ($C_7H_6O_3$) were tested, covering a wide range: 0.05, 0.1, 0.5, 1, 2, 5, 10, 20, 50, 100 and 500×10^{-3} M. Figure 1 shows the structure of the 3-HBA compound.

A mixture of 75 g l^{-1} H_2SO_4, 25 g l^{-1} HF, 30 g l^{-1} H_2O_2 and vol. 5% p-toluene sulphonic acid monohydrate, PTSA, ($C_7H_8O_3S \cdot H_2O$) at pH 2.4 was used as the pickling test solution. All the chemicals were reagent grade.

A polytetrafluroethylene electrochemical cell of 125 ml volume was used with a distilled water flow of 3.4 ml h^{-1}. This device has been described elsewhere [7]. A three-electrode cell arrangement was used for the polarisation tests, with a platinum gauze (~36 cm^2 surface area) as counter electrode, a saturated calomel electrode (SCE) as reference and an AISI 316L SS working electrode with a surface area of 1 cm^2. Polarisation measurements were performed with an EG&G PARC, model 273A, potentiostat at a potential scan rate of 0.16 mV s^{-1}. The temperature was maintained at 298 and 313 K during experimentation. The experiments were conducted after 15 min exposure to the pickling test solution, when the open circuit potential had reached a steady state. This limited time period prevented the dilution of the pickling test solution. To determine the corrosion rates (i_{corr}, current density) the anodic and cathodic Tafel regions were extrapolated to the corrosion potential (E_{corr}).

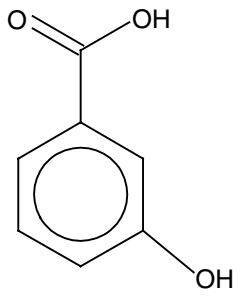

Fig. 1. Molecular structure of 3-HBA inhibitor.

3. Results and discussion

Figures 2 and 3 show polarisation curves for AISI 316L SS in the H_2SO_4–HF–H_2O_2 pickling test solution mixture at 298 and 313 K, respectively, in the presence and absence of 3-HBA inhibitor. It can be observed that AISI 316L SS dissolution shows Tafel behaviour. In general, the dissolution of the SS decreases as the 3-HBA concentration increases. This behaviour may be attributed to an increase in surface coverage (θ) due to adsorption of the inhibitor on the AISI 316L SS surface as the inhibitor concentration increases. Raising the temperature from 298 to 313 K has a positive influence on AISI 316L SS dissolution. It should be noted that no pitting corrosion is observed on the AISI 316L SS surface by polarisation measurements in the presence and absence of inhibitor. Table 1 Includes i_{corr}, coverage (θ) and E_{corr} as a function of 3-HBA concentration.

Comparison of the experimental electrochemical data (θ_{exp} and c_{exp}) and data predicted by a theoretical adsorption equation (θ_{cal} and c_{cal}) is frequently used as the criteria for assessing the validity of a theoretical expression to describe the adsorption equilibrium; where θ has been defined above and c is the concentration of the 3-HBA inhibitor. The θ value was obtained using the expression:

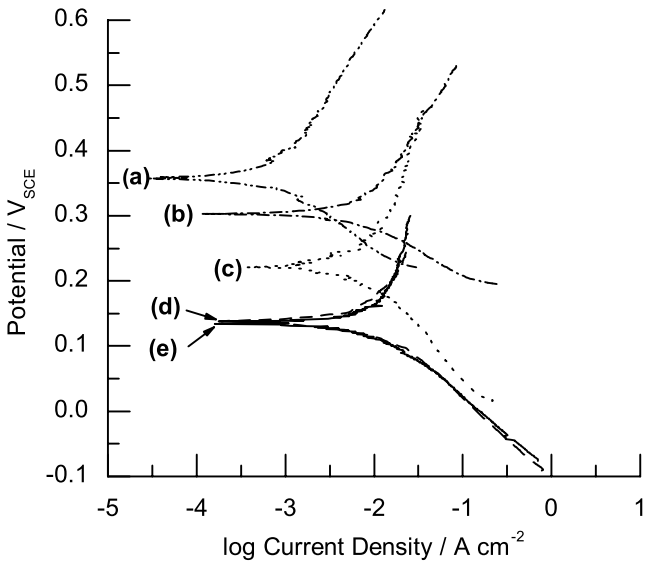

Fig. 2. Polarisation curves for AISI 316L SS in H_2SO_4–HF–H_2O_2 mixture at 298 K: (a) ···· 5×10^{-2} M 3-HBA; (b) –·– 5×10^{-3} M 3-HBA; (c) - - - 2×10^{-3} M 3-HBA; (d) – – 5×10^{-5} M 3-HBA; (e) ———— without 3-HBA.

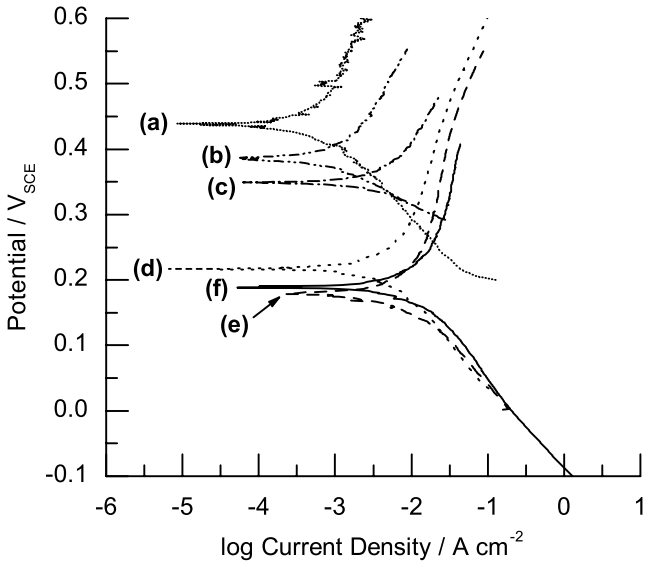

Fig. 3. Polarisation curves for AISI 316L SS in H_2SO_4–HF–H_2O_2 mixture at 313 K: (a) ··· 5×10^{-2} M 3-HBA; (b) –·–· 2×10^{-2} M 3-HBA; (c) –·– 1×10^{-2} M 3-HBA; (d) — 5×10^{-3} M 3-HBA; (e) – – 5×10^{-4} M 3-HBA; (f) ———— without 3-HBA.

Table 1. Current density (i_{corr}) extrapolated from polarisation curves as function of 3-HBA concentration, coverage (θ) obtained using Equation (2), and corrosion potential (E_{corr})

3-HBA concentration (M)	i_{corr}/A cm^{-2}	Coverage (θ)	E_{corr}/V_{SCE}
298 K			
0	1.21×10^{-2}	0	0.134
5×10^{-5}	1.20×10^{-2}	0.008	0.138
1×10^{-4}	1.19×10^{-2}	0.018	0.144
5×10^{-4}	1.14×10^{-2}	0.057	0.144
1×10^{-3}	1.13×10^{-2}	0.073	0.169
2×10^{-3}	9.65×10^{-3}	0.205	0.221
5×10^{-3}	7.20×10^{-3}	0.407	0.303
1×10^{-2}	3.10×10^{-3}	0.745	0.357
2×10^{-2}	1.89×10^{-3}	0.844	0.368
5×10^{-2}	8.01×10^{-4}	0.934	0.380
1×10^{-1}	3.28×10^{-4}	0.973	0.408
5×10^{-1}	2.43×10^{-5}	0.998	0.427
313 K			
0	1.05×10^{-2}	0	0.188
5×10^{-5}	1.04×10^{-2}	0.010	0.229
1×10^{-4}	1.03×10^{-2}	0.019	0.172
5×10^{-4}	1.01×10^{-2}	0.031	0.178
1×10^{-3}	9.43×10^{-3}	0.098	0.191
2×10^{-3}	8.22×10^{-3}	0.214	0.226
5×10^{-3}	6.04×10^{-3}	0.423	0.216
1×10^{-2}	2.44×10^{-3}	0.767	0.347
2×10^{-2}	1.19×10^{-3}	0.886	0.386
5×10^{-2}	7.53×10^{-4}	0.928	0.439
1×10^{-1}	1.67×10^{-4}	0.984	0.452
5×10^{-1}	1.05×10^{-5}	0.999	0.463

$$\theta = \frac{i_{corr_{abs}} - i_{corr_{pre}}}{i_{corr_{abs}} - i_{corr_{max}}} \quad (1)$$

where $i_{corr_{abs}}$ and $i_{corr_{pre}}$ are the AISI 316L SS current densities in the absence and presence of 3-HBA, respectively, and $i_{corr_{max}}$ is the current density for the maximum of inhibition. Considering that $i_{corr_{abs}} >> i_{corr_{max}}$, for a low polarised electrode the Equation (1) can be simplified to the following expression [8, 9]:

$$\theta = \frac{i_{corr_{abs}} - i_{corr_{pre}}}{i_{corr_{abs}}} \quad (2)$$

It should be noted that inhibitor efficiency (IE), as a %, is related to θ by: IE = $\theta \times 100$. Equation (2) is valid based on the assumption that: (a) the adsorption sites on the AISI 316L SS surface are homogeneous, (b) a monolayer inhibitor adsorption is formed, and (c) dissolution is uniform and no localised attack takes place. The c_{cal} value is obtained by evaluation of the theoretical isotherm for a value of θ_{exp} and given the values of k, f and/or χ parameters of the utilised isotherm (see Table 2) [10–17]; k is the equilibrium constant of the adsorption reaction:

$$\text{AISI 316L SS} + \text{3-HBA} \Leftrightarrow \text{AISI 316L SS(3-HBA)}_{ads} \Leftrightarrow \text{AISI 316L}^{n+} + ne^- + \text{3-HBA} \quad (3)$$

given by $k = \left(\frac{1}{55.5}\right)\left[\exp\left(\frac{-\Delta G^0_{ads}}{RT}\right)\right]$; AISI 316L SS (3-HBA)$_{ads}$ is a reaction intermediate. The value 55.5 is the water concentration in the solution in M, R is the gas constant (8.314 J mol^{-1} K^{-1}), T is the absolute temperature and $\Delta G^0{}_{ads}$ is the adsorption energy; f is the interaction term parameter ($f > 0$ lateral attraction between the adsorbed organic molecules and $f < 0$ repulsion between the adsorbed organic molecules); and χ is the number of water molecules replaced by one molecule of 3-HBA (also referred to as the size ratio parameter):

$$\text{3-HBA}_{aqu} + \chi H_2O_{ads} \Leftrightarrow \text{3-HBA}_{ads} + \chi H_2O_{aqu} \quad (4)$$

where 3-HBA$_{aqu}$ is the 3-HBA inhibitor in the aqueous phase, and χH_2O_{ads} is the number of water molecules adsorbed on the AISI 316L SS surface; χ is assumed to be independent of the coverage or charge on the electrode.

The best fit for a given theoretical isotherm is obtained when there is minimal difference between the experimental and calculated values. The expression used to optimise this difference is the objective function (F):

$$F = \sum_{i=1}^{p} w_i \left[c_{exp_i} - c_{cal_i}(k, f, \chi)\right]^2 \quad (5)$$

where the i subscript represents one value in a set of p concentrations of the 3-HBA inhibitor ($1 \le i \le p$), and w_i denotes the weight associated with the i-th experimental value. Ideally, w_i should be the inverse variance of the individual measurements. The next step is to choose the appropriate parameters k, f and/or χ to ensure that Equation (5) has the minimum value.

Because Equation (5) is non-linear, the fitting of such models requires an iterative approach, which may either fail to converge or converges to a local minimum. It is always desirable to carry out the fitting with two or

Table 2. Adsorption isotherms used

Author [Ref.]	Isotherm	Derivative, $\frac{d\log(c)}{d\theta}$
Langmuir [10]	$kc = \frac{\theta}{1-\theta}$	$\frac{1}{\ln(10)}\left[\frac{1}{(1-\theta)\theta}\right]$
Frumkin [11]	$kc = \left(\frac{\theta}{1-\theta}\right)\exp(-f\theta)$	$\frac{1}{\ln(10)}\left[\frac{1}{(1-\theta)\theta} - \mathrm{f}\right]$
Hill-de Boer [12, 13]	$kc = \left(\frac{\theta}{1-\theta}\right)\exp\left(\frac{\theta}{1-\theta}\right)\exp(-\mathrm{f}\theta)$	$\frac{1}{\ln(10)}\left[\frac{1}{(1-\theta)\theta} + \frac{1}{(1-\theta)^2} - \mathrm{f}\right]$
Parsons [14]	$kc = \left(\frac{\theta}{1-\theta}\right)\exp\left[\frac{2-\theta}{(1-\theta)^2}\right]\exp(-\mathrm{f}\theta)$	$\frac{1}{\ln(10)}\left[\frac{1}{(1-\theta)\theta} + \frac{3-\theta}{(1-\theta)^3} - \mathrm{f}\right]$
Damaskin–Parsons [15]	$kc = \frac{\theta}{(1-\theta)^\chi}\exp(-f\theta)$	$\frac{1}{\ln(10)}\left[\frac{1}{(1-\theta)\theta} + \frac{\chi-1}{1-\theta} - \mathrm{f}\right]$
Kastening–Holleck [16]	$kc = \frac{\theta}{\chi(1-\theta)^\chi}\left(1-\theta+\frac{\theta}{\chi}\right)^{(\chi-1)}\exp(-f\theta)$	$\frac{1}{\ln(10)}\left[\frac{1}{(1-\theta)\theta} + \frac{\chi-1}{1-\theta} - \frac{(\chi-1)^2}{\chi}\left(1-\theta+\frac{\theta}{\chi}\right)^{-1} - \mathrm{f}\right]$
Flory–Huggins [15]	$kc = \frac{\theta}{\chi(1-\theta)^\chi}$	$\frac{1}{\ln(10)}\left[\frac{1}{(1-\theta)\theta} + \frac{\chi-1}{1-\theta}\right]$
Dhar–Flory–Huggins [15]	$kc = \frac{\theta}{(1-\theta)^\chi\exp(\chi-1)}$	$\frac{1}{\ln(10)}\left[\frac{1}{(1-\theta)\theta} + \frac{\chi-1}{1-\theta}\right]$
Bockris–Swinkels [17]	$kc = \frac{\theta}{(1-\theta)^\chi}\frac{[\theta+\chi(1-\theta)]^{(\chi-1)}}{\chi^\chi}$	$\frac{1}{\ln(10)}\left[\frac{1}{(1-\theta)\theta} + \frac{\chi-1}{1-\theta} - \frac{(\chi-1)^2}{\chi}\left(1-\theta+\frac{\theta}{\chi}\right)^{-1}\right]$

more separate and quite differentiated initial parameter value sets. If two or more of them converge to the same final parameter set, it is reasonable to assume that the least squares solution has been obtained. Fitting has been carried out using the Levenberg–Marquardt algorithm to minimise the F.

Figure 4 shows coverage (θ) versus concentration of 3-HBA inhibitor for AISI 316L SS immersed in the 75 g l^{-1} H_2SO_4, 25 g l^{-1} HF, 30 g l^{-1} H_2O_2 and vol. 5% PTSA test solution mixture at 298 K. The value of θ was calculated using the Equation (2). The figure also includes simulated data using the Frumkin equation (see Table 2), with $f = 1.57$ and $k = 84.3$, where f and k parameters were obtained using the preceding non-linear fitting; and $f = 1.23$, and $k = 122.62$, where f and k parameters were obtained using linear fitting.

The aim of a linear regression method is to find the best straight line described by a set of points. If the behaviour of the experimental data in Figure 4 is described by the Frumkin equation, it is obvious that the data cannot be fitted to a straight line. However, it is possible to carry out mathematical transformations of the experimental data in order to achieve a straight line fit. For instance, considering the Frumkin equation it is possible to find the following expression:

$$\ln\left(\frac{\theta}{c(1-\theta)}\right) = f\theta + \ln(k) \tag{6}$$

which is the equation of a straight line with an ordinate origin [$\ln(k)$] and the slope (f).

Figure 5 shows a $\ln\left(\frac{\theta}{c(1-\theta)}\right)$ versus θ plot using the experimental data shown in Figure 4. Figure 5 also includes the straight line (solid line) obtained using linear fitting. The $f = 1.23$ and $k = 122.62$ parameters of the Frumkin equation in Figure 4 were obtained using this procedure.

The two procedures described above should, in principle, supply identical results. However, as can be seen in Figure 4, non-linear fitting (solid line) is more appropriate than linear fitting (broken line). A possible explanation for this is that the mathematical transformations of the experimental data introduce some errors.

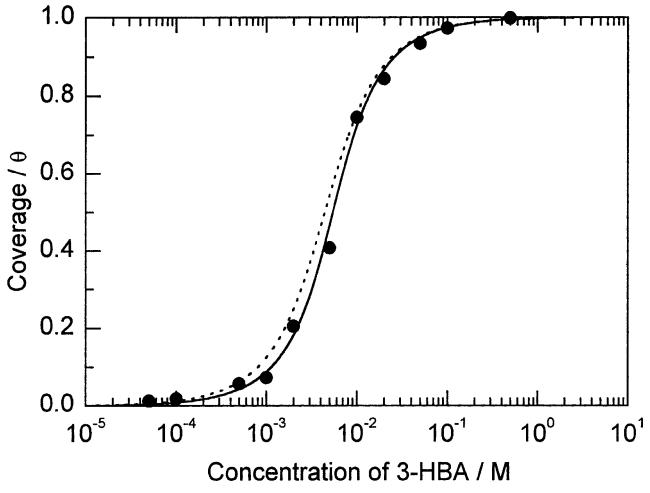

Fig. 4. Coverage versus 3-HBA concentration for AISI 316L SS in H_2SO_4–HF–H_2O_2 mixture at 298 K: ● experimental, – – linear fitting ($f = 1.23$ and $k = 122.62$), ——- non-linear fitting ($f = 1.57$ and $k = 84.3$).

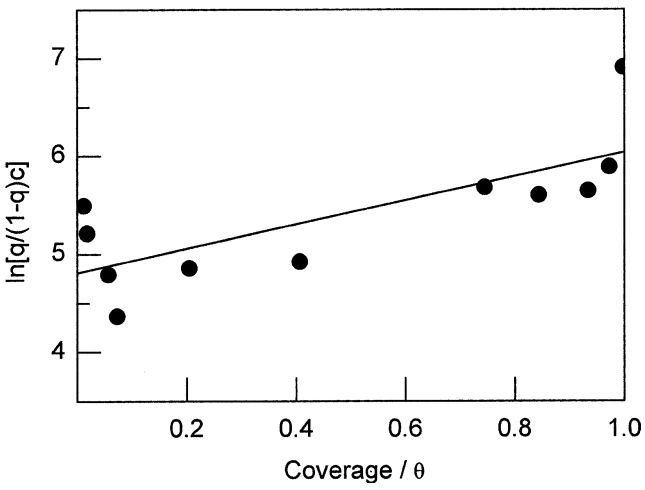

Fig. 5. Representation of $\ln[\theta/c(1-\theta)]$ versus 3-HBA coverage for AISI 316L SS in H_2SO_4–HF–H_2O_2 mixture at 298 K: ● experimental, ———— linear fitting.

Linear fitting assumes that: (i) the scattering of the experimental data follows a Gaussian distribution, and (ii) the standard deviation is the same for each data. In general, these hypotheses cannot be applied after the mathematical transformations of the experimental data. Thus, the ordinate origin [ln(k)] and the slope (f) values, Equation (6), obtained from Figure 5 do not seem to be the most reliable way to obtain the Frumkin equation parameters: k and f.

In order to study the adsorption of 3-HBA on AISI 316L SS electrode surfaces, the properties of the isotherm equations from Table 2: the shape, the trend of the slopes along the curve, and the existence of inflection points, were analysed as the characteristics that differentiate one adsorption equation from another.

The Langmuir slope, $\ln(10)(1-\theta)\theta$ (see Table 2), shows that, for a given value of θ, the slope has a constant value, regardless of the value of k. The term $(1-\theta)\theta$ is a parabolic function with a maximum at $\theta = 0.50$. Thus, the criterion for identifying Langmurian behaviour in a θ versus log(c) plot lies in the characteristic slopes of the curves.

Figure 6 shows the slope of the Frumkin equation, $\frac{\mathrm{d}\log(c)}{\mathrm{d}\theta} = \frac{1}{\ln(10)}\left[\frac{1}{(1-\theta)\theta} - f\right]$, as a function of θ for AISI 316L SS immersed in the H_2SO_4–HF–H_2O_2 aqueous mixture in the presence of 3-HBA at 298 and 313 K temperatures. A cubic spline polynomial algorithm was used to interpolate the data in the unmeasured 3-HBA concentration domain between each pair of experimental data and to obtain the derivative (d log(c)/dθ) for a continuous function [18, 19]. Attractive interactions between inhibitor molecules ($f > 0$) can be directly identified by observing the slope at intermediate coverage values. The slope of the Frumkin equation is steeper than that of the Langmuir equation, and the deviation is due to a positive f value. For repulsive interactions ($f < 0$) the slope of the Frumkin equation is less steep than that of the Langmuir equation. For the case where $f = 0$, the slope of the Frumkin equation is simplified to the slope of the Langmuir equation (see Table 2). This means that, compared with the Langmuir equation, in the Frumkin equation the slope is modified by a constant value f. This effect is shown graphically in the theoretical inset of Figure 6.

Figure 6 inset also shows that the Langmuir equation ($f = 0$) exhibits a minimum slope for intermediate coverage. At high or low coverage the slope values are determined by the term $\frac{1}{(1-\theta)\theta}$, which dominates whenever $\frac{1}{(1-\theta)\theta} \gg f$. Thus, f is only able to modify the slope at intermediate coverage values (when $\frac{1}{(1-\theta)\theta} \sim f$) by shifting the Langmuir slope by a constant value of f. This shift can be positive (rising) for $f < 0$ or negative (falling) for

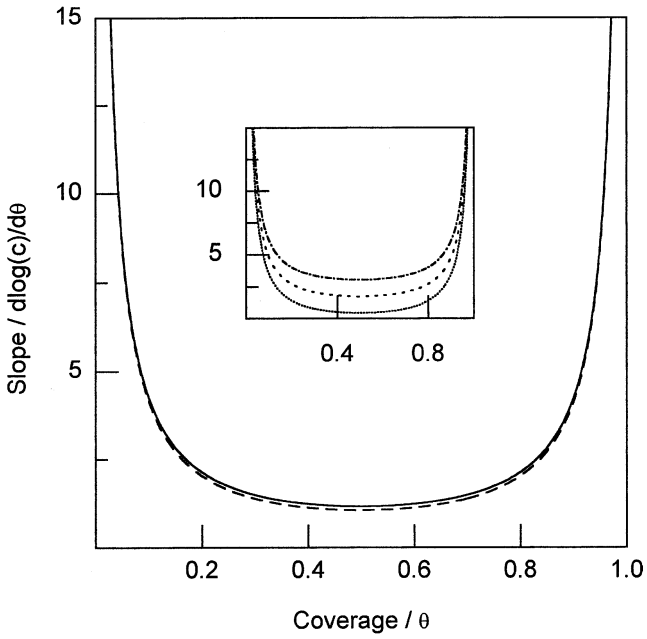

Fig. 6. Slope versus coverage using Frumkin equation: – – 298 K; ——— 313 K. Inset: ···· $f = +3$; – – $f = 0$; –·– $f = -3$.

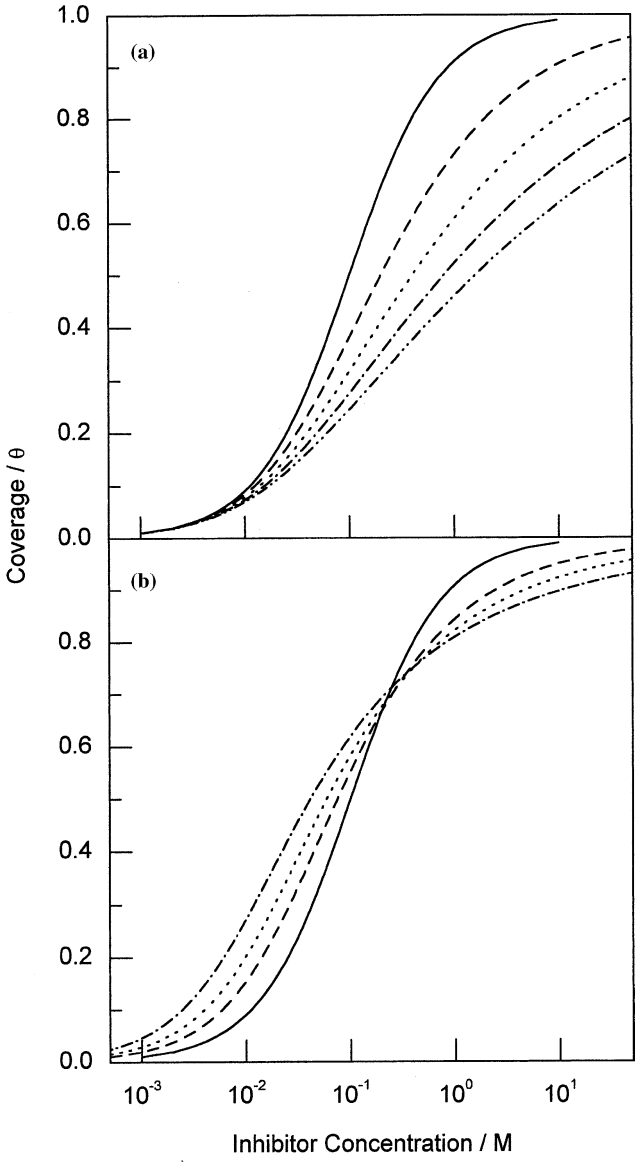

Fig. 7. Coverage versus inhibitor concentration for: ——— $\chi = 1$; – – $\chi = 2$; ···· $\chi = 3$; –·– $\chi = 4$; –··– $\chi = 5$, using (a) Damaskin–Parsons equation, and (b) Kastening–Holleck equation.

$f > 0$ (see Figure 6 inset). This property is not exclusive to the Frumkin equation, and can be extended to any adsorption isotherms which include the $\exp(-f\theta)$ term, e.g. Hill-de Boer, Parsons, Damaskin–Parsons and Kastening–Holleck equations (see Table 2).

Adsorption equations that contain the χ parameter have the overall effect of depressing an adsorption curve. This is shown for the Damaskin–Parsons equation in the theoretical plot of Figure 7a and for the Kastening–Holleck equation in the theoretical plot of Figure 7b. Due to the similarities between the Kastening–Holleck and Bockris–Swinkels equations, the latter follows a similar pattern to Figure 7b. In fact, the slope of the Bockris–Swinkels equation is a particular case: $f = 0$ in the Kastening-Holleck equation (see Table 2).

The derivative of the Damaskin–Parsons equation is identical to the Frumkin slope, apart from the term: $\frac{\chi-1}{1-\theta}$ (see Table 2). Figure 8 shows the theoretical variation in the slope of the Damaskin-Parsons equation, $\frac{\mathrm{d}\log(c)}{\mathrm{d}\theta} = \frac{1}{\ln(10)}\left[\frac{1}{(1-\theta)\theta} + \frac{\chi-1}{1-\theta} - f\right]$, as a function of θ. It can be observed that the contribution of the term $\frac{\chi-1}{1-\theta}$ increases as the value of θ rises and is responsible for the overall depression of the adsorption equation curve.

The derivative of the Kastening–Holleck equation is identical to the Damaskin–Parsons slope, apart from the term: $-\frac{(\chi-1)^2}{\chi}\left(1-\theta+\frac{\theta}{\chi}\right)^{-1}$ (see Table 2). The latter term is the least important, and affects the low coverage region. The minimum of the slope values in Figure 8 serves as a criterion for distinguishing between compounds that adsorb according to the χ-parameter and those that adsorb according to the Frumkin and Langmuir equations, which show a constant inflection point (θ_{ip}) at $\sim$0.50.

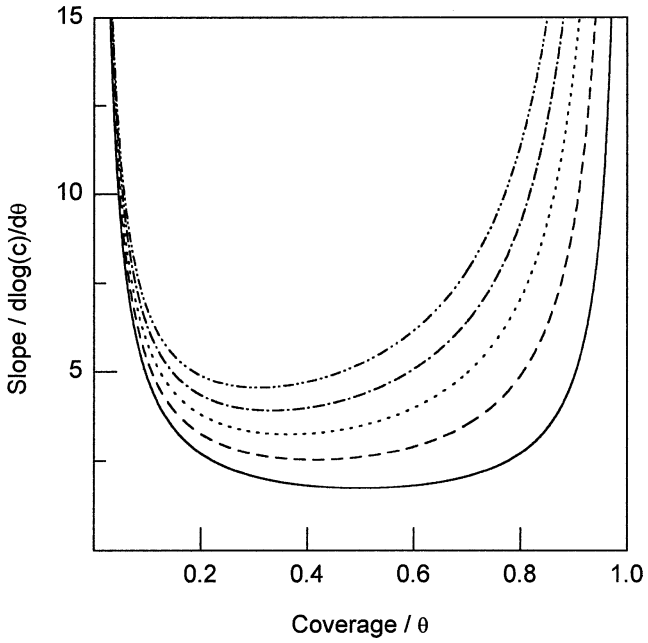

Fig. 8. Slope versus coverage for $f = 0$ using Damaskin–Parsons equation: ——— $\chi = 1$; – – $\chi = 2$; ···· $\chi = 3$; –·– $\chi = 4$; –··– $\chi = 5$.

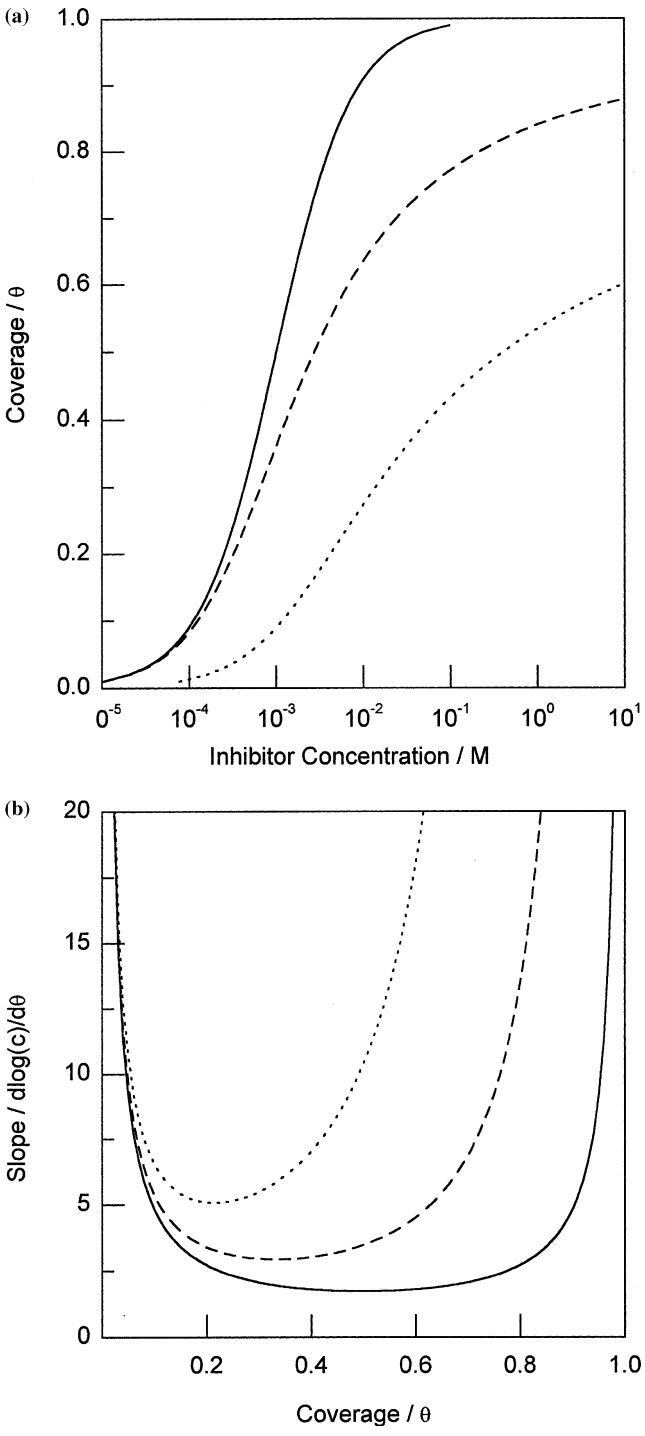

Fig. 9. Fitting using: ——— Frumkin equation, – – Hill-de Boer equation, and ···· Parsons equation. (a) Coverage versus inhibitor concentration for $f = 0$ and $k = 1000$. (b) Slope versus coverage for $f = 0$.

The two-parameters (k and f) in the Hill-de Boer and Parsons equations are similar to the Frumkin equation. They produce sigmoid curves with distinctive θ_{ip} at 0.33 and 0.21 for the Hill-de Boer and Parsons equations, respectively (see Figure 9a). This feature can be appreciated from their derivatives, see Table 2. Figure 9b shows $\mathrm{d}\log(c)/\mathrm{d}\theta$ as a function of θ using the Frumkin, Hill-de Boer and Parsons equations. The minima correspond to the θ_{ip} of the slope, which is characteristic

of each equation and independent of the k and f parameters. Finally, the Hill-de Boer and Parsons equations are depressed curves, and the slopes of the isotherms are sensitive to f changes for $\theta \sim\theta_{ip}$.

The derivatives of the Flory–Huggins and Dhar–Flory–Huggins equations are identical to the derivative of the Damaskin–Parsons equation, apart from the term: f (see Table 2).

From the preceding discussion it is concluded that the Frumkin equation best describes the adsorption of the 3-HBA compound on a AISI 316L SS electrode surface in the presence of the H_2SO_4–HF–H_2O_2 aqueous pickling solution at 298 K. The discussion is now centred on results using the Frumkin isotherm.

Figure 10 shows the degree of coverage versus 3-HBA inhibitor concentration for AISI 316L SS in 75 g l^{-1} H_2SO_4, 25 g l^{-1} HF, 30 g l^{-1} H_2O_2 and vol. 5% PTSA test solution mixture at 313 K temperature. Figure 4 (solid line) shows the results at 298 K. These figures also display the simulated data using the Frumkin equation. The curves in Figures 4 and 10 have an S shape, as predicted by the Frumkin equation, defining three regions on the isotherm plot: (a) at low 3-HBA concentration an increase in the inhibitor concentration does not produce an increase in θ, (b) at intermediate 3-HBA concentrations a small increase in the inhibitor concentration causes a high θ (a linear dependence of θ versus log(c)), and (c) at high 3-HBA concentrations θ is independent of the inhibitor concentration. A positive value of f has been associated with a vertical orientation of the inhibitor molecule on an electrode surface [20].

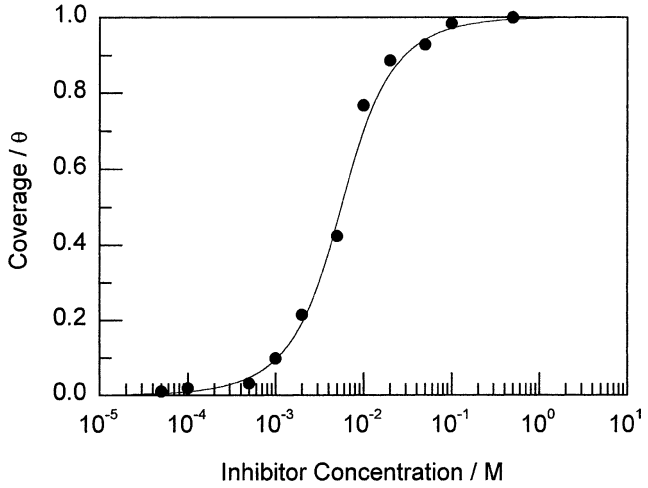

Fig. 10. Coverage versus 3-HBA concentration for AISI 316L SS in H_2SO_4–HF–H_2O_2 mixture at 313 K using Frumkin equation: ● experimental, ——— simulated.

Table 3. Thermodynamic data for AISI 316L SS in H_2SO_4–HF–H_2O_2 mixture in the presence of 3-HBA using the Frumkin equation

Temperature (K)	f	ΔG^0_{ads}/kJ mol^{-1}	k
298	1.57	−20.97	84.3
313	1.32	−22.24	92.7

Table 3 includes f, ΔG^0_{ads} and k parameters from Figures 4 and 10. The value of f is non-zero and, consequently, is further proof that the adsorption mechanism cannot be related by the Langmuir model. The f parameter values are positive. The small and positive value of parameter f indicates weak attraction between the adsorbed molecules. The negative value of ΔG^0_{ads} indicates that the reaction proceeds spontaneously. The k parameter increases as the temperature rises, i.e. this parameter produces electrical interactions between the double layer existing at the phase boundary and the adsorbing molecules.

The inhibition mechanism of 3-HBA may be explained by the AISI 316L SS $(3\text{-HBA})_{ads}$ reaction intermediates, see Equation (3). At first, when there is not enough AISI 316L SS $(3\text{-HBA})_{ads}$ to cover the AISI 316L SS surface, because the inhibitor concentration is low or because the adsorption rate is slow, metal dissolution takes place at sites on the AISI 316L SS surface free of $(3\text{-HBA})_{ads}$ species. With a high 3-HBA concentration a compact and coherent inhibitor overlayer is formed on the AISI 316L SS which reduces chemical attack on the metal. As the surface of AISI 316L SS is basically hydrophobic, the COOH and OH functional groups are unlikely to be oriented towards the surface. In contrast, the hydrophobic corners of the ring are probably more prone to be in contact with the

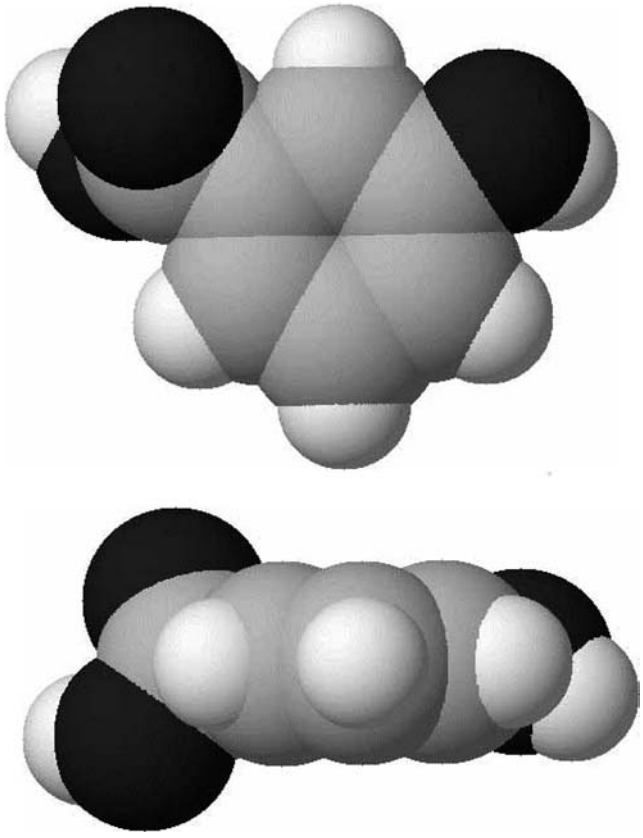

Fig. 11. Front view of 3-HBA molecule adsorbed onto AISI 316L SS electrode in horizontal orientation (top) and in vertical orientation (bottom).

surface due to the π-electrons system being capable of donating electron pairs to metal atoms.

Finally, in order to calculate the optimal orientation of 3-HBA for adsorption on the AISI 316L SS electrode surface, the projected molecular surface area of 3-HBA was calculated using molecular models. Figure 11 (top) shows that the area occupied by a horizontally oriented adsorbed 3-HBA molecule is ~41 $Å^2$ (the projected area of a rectangle surrounding a molecule), compared with ~25 $Å^2$ for the vertical orientation (Figure 11, bottom). These values were obtained after configuration calculations using the value of Van der Waal's atomic radii [21]. The area occupied by a vertically adsorbed water molecule is in the range 8–12 $Å^2$ [22]. Thus, a vertical orientation of 3-HBA displaces two or three water molecules ($\chi \sim 2$–3) while a horizontal orientation of 3-HBA displaces 4–5 water molecules. The apparent contradiction in the displacement of more than one water molecule using the Frumkin equation has been attributed to the fact that one adsorption site on the AISI 316L SS electrode surface is occupied by a group of associated water molecules [23].

4. Conclusions

AISI 316L stainless steel corrosion rate was obtained in a H_2SO_4–HF–H_2O_2 aqueous solution mixture in the presence and absence of 3-HBA as corrosion inhibitor, at temperatures of 298 and 313 K, using polarisation curves. The AISI 316L stainless steel corrosion rate increased with the temperature, this being an effect of particular significance at low 3-HBA inhibitor concentrations. An improvement in inhibitor efficiency was observed as a function of increasing 3-HBA concentration.

The inhibitor mechanism was analysed for the most common isotherm equations used in corrosion studies, in terms of the shape (sigmoid curve); the trend of the slopes along the curve, depending on the interaction term (f) parameter and the configurational term (χ) parameter; and the existence of an inflection point (θ_{ip}), for instance, $\theta_{ip} \sim 0.50$ for the Langmuir and Frumkin equations, $\theta_{ip} \sim 0.33$ for the Hill-de Boer equation, and $\theta_{ip} \sim 0.21$ for the Parsons equation. The Frumkin equation best described the adsorption of the 3-HBA compound on a AISI 316L stainless steel surface in the presence of the H_2SO_4–HF–H_2O_2 aqueous pickling solution.

The projected molecular surface area method was a good approach for correlating the effectiveness of a film-forming of 3-HBA corrosion inhibitor on AISI 316L stainless steel.

Acknowledgements

The authors wish to express their gratitude to the CYCIT of Spain for financial support under Project No. MAT2001-1732-C02-01, and to ACERINOX for supplying the AISI 316L stainless steel used.

References

1. C.D. Dillon, *Mater. Performance* **33** (1994) 62.
2. A.M. Al-Mayouf, A.K. Al-Ameery and A.A. Al-Suhybani, *Br. Corros. J.* **36** (2001) 127.
3. Chief Inspector's Guidance to Inspector, Guidance Note IPR 4/11, HMSO, London (1993).
4. N.J. Sanders, *Anti-Corros Method. M.* **44** (1997) 20.
5. J. Seppala, S. Koskela, M. Melanen and M. Palperi, *Resour. Conserv. Recy.* **35** (2002) 61.
6. L. Narváez, E. Cano and J.M. Bastidas, *Mater. Corros.* **54** (2003) 84.
7. J.M. Bastidas, C. Fosca, B. Chico and E. Otero, *Mater. Corros.* **48** (1997) 216.
8. A.N. Frumkin and B.B. Damaskin, in Modern Aspects of Electrochemistry. J.O'M. Bockris and B.E. Conway (Ed), Vol. 3 Plenum PressNew York, p. 149.
9. I.A. Ammar and F.M. El-Khorafi, *Werkst. Korros.* **24** (1973) 702.
10. I. Langmuir, *J. Am. Chem. Soc.* **40** (1918) 1361.
11. A.N. Frumkin, *Z. Phys. Chem.* **116** (1925) 466.
12. T.L. Hill, *J. Chem. Phys.* **20** (1952) 141.
13. J.H. de Boerde, *The Dynamical Character of Adsorption* (Oxford University Press, Oxford, 1953).
14. R. Parsons, *J. Electroanal. Chem.* **8** (1964) 93.
15. B.B. Damaskin, O.A. Petrii and V.V. Batrakov, 'Adsorption of Organic Compounds on Electrodes', Plenum Press, New York, 1971), pp. 86, 94 and 247.
16. B. Kastening and L. Holleck, *Talanta* **12** (1965) 125.
17. J.O'M. Bockris and D.A.J. Swinkels, *J. Electrochem. Soc.* **111** (1964) 736.
18. J.M. Bastidas, J.L. Polo, C.L. Torres and E. Cano, *Corros. Sci.* **43** (2001) 269.
19. J.M. Bastidas, M. Saiki, S.O. Rogero, I Costa and J.L. Polo, *J. Appl. Electrochem.* **23** (2002) 487.
20. J.M. Bastidas, J. Damboreneade and A.J. Vazquez, *J. Appl. Electrochem.* **27** (1997) 345.
21. J.M. Bastidas, J.L. Polo and E. Cano, *J. Appl. Electrochem.* **30** (2000) 1173.
22. J.M. Bastidas, J.L. Polo, E. Cano and C.L. Torres, *J. Mater. Sci.* **35** (2000) 2637.
23. B.B. Damaskin and G.A Tedoradze, *Electrochim. Acta* **10** (1965) 529.